Flow Past Airfoil Moving Reciprocally in a Channel by Vortex Method

Ki-Deok Ro*

School of Mechanical and Aerospace Engineering · Institute of Marine Industry, Gyeongsang National University, 445 Inpyeong-dong, Tongyeong, Gyeongnam 650-160, Korea

The velocity and pressure fields of a ship's propulsion mechanism of the Weis-Fogh type, in which a airfoil moves reciprocally in a channel, are studied in this paper using the advanced vortex method. The airfoil and the channel are approximated by a finite number of source and vortex panels, and the free vortices are introduced from the body surfaces. The viscous diffusion of fluid is represented using the core-spreading model to the discrete vortices. The velocity is calculated on the basis of the generalized Biot-Savart law and the pressure field is calculated from integrating the equation given by the instantaneous velocity and vorticity fields. Two-dimensional unsteady viscose flows of this propulsion mechanism are numerically clarified, and the calculated results agree well with the experimental ones.

Key Words : Computational Fluid Dynamics, Vortex Method, Propulsion Mechanism, Unsteady Flow

1. Introduction

The Weis-Fogh mechanism, discovered through the analysis of wing motion in the hovering flight of a small bee called Encarsia Formosa, is a novel and very efficient mechanism for lift generation (Weis-Fogh, 1973 ; Lighthill, 1973). In the flight of this tiny bee, the beating rate of the wings is about 400 Hz, and the Reynolds number R_e, defined by the wing chord and mean velocity of the leading edge, is approximately 30. The lift coefficient (C_L) is approximately 3~4 for the bee' s wing, which is much higher than the lift coefficient that would be calculated for this wing in steady flow. This means that the insect efficiently generates lift using unsteady wing motion.

* **E-mail** : rokid@gaechuk.gsnu.ac.kr
TEL : +82-55-640-3123; **FAX** : +82-55-640-3128
School of Mechanical and Aerospace Engineering · Institute of Marine Industry, Gyeongsang National University, 445 Inpyeong-dong, Tongyeong, Gyeongnam 650-160, Korea. (Manuscript **Received** November 17, 2005; **Revised** May 17, 2006)

Tsutahara (1987 ; 1989) presented the propulsion model, which used the two-dimensional model of the Weis-Fogh mechanism in a water channel, and showed that this propulsive device operates very effectively by conducting experiments on the dynamic characteristics, and a working test on a model ship as the new ship propulsion system. Ro (2000) simulated the unsteady flow fields by applying the conventional discrete vortex method on the perimeter of the wing while the propulsive mechanism was being operated, and also verified the time variation of the thrust and the drag on the wing. Due to assumptions in the simulation of potential flows without viscosity and a consideration of the wing as a plate without thickness, these numerical predictions have limitations compared with the experimental results.

This paper, therefore, clearly verifies the velocity and pressure fields in the Weis-Fogh type ship propulsion mechanism using the advanced vortex method (Kamemoto, 1995), and contributes to its practical application as a propulsion system.

2. Numerical Method

2.1 A model of a propulsion device

Figure 1 shows the analytical model of a Weis-Fogh type ship propulsion mechanism. Perpendicularly, the figure shows the upper part of the model, and, as a wing in the water channel oscillates in a reciprocal operation, the propulsive power rises to the left (the direction towards which the ship is progressing). This model is identical to the Tsutahara et al. model (1987), and so a brief synopsis of it will be sufficient.

A wing is installed in a square channel. When the point p corresponding to the center axis of the wing is oscillated back and forth along the y-axis, the wing first opens at point p from the lower surface (opening stage). Then, maintaining an open angle α, the wing moves translationally in a parallel movement (translating stage), and finally rotates and closes on the upper surface (closing stage) through the reciprocal motion of point p. It then executes an opening stage at the upper surface once more, moves translationally once again, and repeats the closing stage at the lower surface.

Originally, in the Weis-Fogh mechanism, circulation in the opposite direction is formed at each wing, as a pair of flat-plate wings open while their trailing edges touch. However, through the principle of a mirror image, when channel walls are in place and the same motions as above are executed by a single wing, as shown in the analytical model of Fig. 1, the identical effects can be achieved with as a pair of wings.

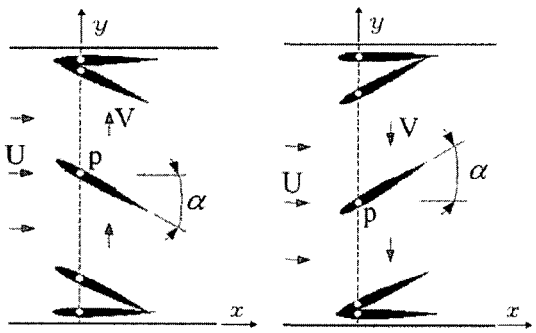

(a) Up stroke (b) Down stroke

Fig. 1 A model of propulsion mechanism

2.2 Introduction of a nascent vortex elements

The model of the Weis-Fogh type propulsion mechanism utilizes the driving system shown in Fig. 1. Comparing it with the results of Ro's experiment (2000), the numerical model was found to have a hydrodynamic similarity with the experimental conditions, and the shape of the wing was also set at NACA0010, as given in the reference.

By calculating the velocity and the pressure field of this propulsion unit during the movement of the wing shown in Fig. 1(a) and 1(b) for every time step, we could examine the results. The movement of the wing at the opening and closing stages is easily represented by combining the translating and rotating motions.

Here, assuming that two flat plates and a wing in the flow field were installed, the surfaces of each object were represented with double panels, that is, with a finite number of source and vortex panels. At this time, the unknowns that should be determined at each time step were the source strength on the panel for M pieces and the circulation around the wing and two walls of the water channel. These unknowns were obtained using the Neumann condition in Eq. (1) at the center of the source panel for M pieces ($i=1, 2, 3, \cdots, M$), and the theorem of Kelvin in Eq. (2) for the circulation of each object perimeter, $\Gamma_b=\gamma_{bs}\cdot S_b$.

$$\left\{\sum_{j=1}^{M}(\boldsymbol{u}^{sp}+\boldsymbol{u}^{vp})_{ij}+\sum_{k=1}^{N}\boldsymbol{u}_{ik}^{vo}+U\right\}\cdot\boldsymbol{n}_i=\boldsymbol{u}_i\cdot\boldsymbol{n}_i \quad (1)$$

$$\Gamma_b+\sum_{k=1}^{N_b}\Gamma_{bk}^{vo}=0 \quad (2)$$

Here $\boldsymbol{u}^{sp}$, $\boldsymbol{u}^{vp}$ and $\boldsymbol{u}^{vo}$ are the induced velocities that were deduced from the source panels, the vortex panels, and the vortex elements introduced into the flow field; U and $\boldsymbol{u}_i$ are the uniform flow and the velocity of the i-th control point; $\boldsymbol{n}_i$ is the unit vector of the vertical direction at the i point; γ_{bs} and S_b represent the circulation per the unit length for each object perimeter and the length of the perimeter; and Γ_{bk}^{vo} is the circulation of the vortex element that is emitted by each

object. Here, assuming that γ_{bs} is constantly distributed around the object, it can be obtained from $\gamma_{bs}=\Gamma_b/S_b$, then $\boldsymbol{u}^{vp}$ is calculated by γ_{bs}.

In the case of the conventional vortex method, this situation was found to be numerically unstable. In this paper, however, by considering a double fold of the source and vortex panels, the above unstable numerical problem could be eliminated.

Figure 2 illustrates the schematic of the thin vorticity layer and the introductory method of the nascent vortex elements. The vorticity field near the solid surface is represented by the proper distribution of the vorticity layers and the discrete vortex elements to satisfy the no-slip condition on the body surface. A thin vorticity layer with thickness h_i was considered along the body surface, and the solid body was discretized by a number of source panels, as shown in Fig. 2.

Assuming that the flow was considered two-dimensional and that there was a linear distribution of the velocity in the thin vorticity layer, and for the simplicity of illustration, suppose the solid is stationary, the normal convective velocity V_c on the outer boundary of the vorticity layer can be expressed using the relation of continuity of flow and the no-slip condition on the solid surface for the element of the vorticity layer [abcd] as:

$$V_c=\frac{1}{s_i}\left\{\frac{h_i u_i}{2}-\frac{h_{i+1}u_{i+1}}{2}\right\} \tag{3}$$

in which s_i, h_i and u_i represent the panel length,

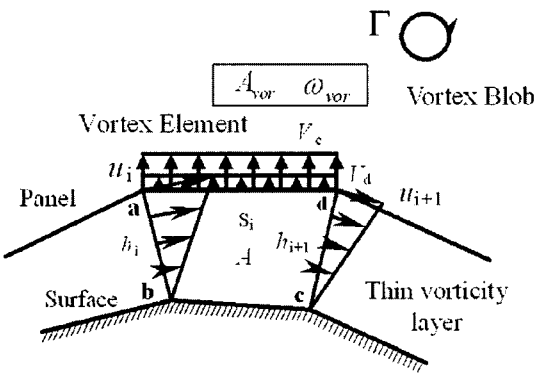

Fig. 2 Thin vorticity layer and nascent vortex element

the thickness of the vorticity layer, and the tangential velocity at each node of outer boundary, respectively. As the solid is movable, Eq. (3) is still valid when u_i is thought of as a velocity relative to the moving solid.

On the other hand, the vorticity of the thin shear layer diffused through the panel into the flow field. In order to consider this vorticity diffusion, we obtain the diffusion velocity V_d at the outer boundary of the vorticity layer as:

$$V_d=\frac{1.136^2\nu}{h_i+h_{i+1}} \tag{4}$$

Here, ν is the kinematic viscosity of the fluid. If the value of (V_c+V_d) becomes positive, a nascent vortex element is introduced in the flow field, where the thickness h_{vor} and ω_{vor} the vorticity of the vortex element are obtained as follows:

$$h_{vor}=(V_c+V_d)\,dt \tag{5}$$

and,

$$\omega_{vor}=\frac{\Gamma}{A+A_{vor}} \tag{6}$$

Here, Γ is the circulation originally involved in the element of the vorticity layer [abcd] calculated according to Eqs. (1) and (2), and A and A_{vor} are the areas of the vorticity layer element and the nascent vortex element. The square-type vortex element generated during each time step is substituted with a vortex blob at a fixed height.

Moreover, as a linear distribution of velocity is assumed in the thin vorticity layer, the shearing stress on the wall surface is approximated from the following equation, as long as the thickness of the vorticity layer is sufficiently thin:

$$\tau_w=\mu\frac{\partial u}{\partial y}=-\mu\omega \tag{7}$$

2.3 Calculation of the velocity field

A trajectory of the vortex shedding element over the time step dt is approximated by applying the following Adams-Bashforth method as:

$$\boldsymbol{r}(t+dt)=\boldsymbol{r}(t)+\{1.5\boldsymbol{u}(t)-0.5\boldsymbol{u}(t-dt)\}\,dt \tag{8}$$

in which the motion $\boldsymbol{u}$ of the vortex element can be derived from the following Biot-Savart law that includes source panels, vortex sheet panels and all vortex elements existing in the flow field.

$$\boldsymbol{u}(\boldsymbol{r})=\frac{1}{2\pi}\int_V \frac{\boldsymbol{\omega}\times\boldsymbol{R}}{R^2}dV-\frac{1}{2\pi}\times\int_{S_0}\left[\frac{(\boldsymbol{n}_0\cdot\boldsymbol{u}_0)\cdot\boldsymbol{R}_0}{R_0^2}-\frac{(\boldsymbol{n}_0\times\boldsymbol{u}_0)\times\boldsymbol{R}_0}{R_0^2}\right]dS_0 \tag{9}$$

In the second term of the RHS in Eq. (9), $\boldsymbol{R}_0$ represents $\boldsymbol{R}_0=\boldsymbol{r}-\boldsymbol{r}_0$ and $R_0=|\boldsymbol{R}_0|$.

The Lagrangian expression for the vorticity transport equation is expressed as:

$$\frac{d\boldsymbol{\omega}}{dt}=(\boldsymbol{\omega}\cdot grad)\,\boldsymbol{u}+\nu\nabla^2\boldsymbol{\omega} \tag{10}$$

where, in a two-dimensional case, the first term of the RHS disappears, and in the second term, the viscous diffusion term remains. This viscous diffusion term is approximated using the core spreading method (Leonard 1980).

$$\varepsilon_k(t+dt)=\varepsilon_k(t)+\frac{2.242^2\nu}{2\varepsilon_k(t)}dt \tag{11}$$

According to Eq. (9), in the flow fields of this propulsion mechanism, the vortex distribution, streak line and velocity field are predicted in each time step, and the streamlines are plotted from the vector field.

2.4 Calculation of the pressure field

If the divergence is applied to the Navier-Stokes equation, the pressure Poisson equation becomes:

$$\nabla^2 p=-\rho div(\boldsymbol{u}\cdot grad\boldsymbol{u}) \tag{12}$$

In general, the pressure field is obtained by calculating the Poisson equation using the finite difference method. In this case, some lattices must be generated in the flow field, such that the merits of the vortex method that the grid generation does not need would be lost. Therefore, in this research, instead of using the finite difference method of the Poisson equation, the pressure in the flow field is obtained from the integration equation formulated by Uhlman (1992), as follows:

$$\beta H+\int_{S_0}H\frac{\partial G}{\partial \boldsymbol{n}}dS_0=-\int_V\nabla(\boldsymbol{u}\times\boldsymbol{\omega})\,dV-\int_{S_0}\left\{G\cdot\boldsymbol{n}\cdot\frac{\partial\boldsymbol{u}}{\partial t}+\nu\cdot\boldsymbol{n}\cdot(\nabla G\times\boldsymbol{\omega})\right\}dS_0 \tag{13}$$

in which $\beta=1$ refers to the inside flow and the boundary surface S_0 is represented by $\beta=1/2$. G is the fundamental solution of the scalar Laplace equation with the delta function expressed as:

$$G=\frac{1}{2\pi}\log\left(\frac{1}{R}\right) \tag{14}$$

and H is the Bernoulli-type variable, defined as follows:

$$H_i=\frac{p_i}{\rho}+\frac{u_i^2}{2} \tag{15}$$

The pressure field of the propulsion mechanism was calculated from the pressure distribution on the body surfaces using Eqs. (13) and (15) during each time step, and with this information, isobaric lines of the entire flow field were taken. By integrating the normal component of the pressure and the tangential component of the shear stress around the wing surface, the hydrodynamic force F acting on the wing was obtained simply using:

$$\boldsymbol{F}=iF_x+jF_y=\oint_{S_0}\{(-p\cdot\boldsymbol{n})+\tau_w\cdot\boldsymbol{t}\}\,dS_0 \tag{16}$$

in which F_x and F_y represent the components of force at the x and y directions, equivalent the thrust T and the drag force D for the negative direction. That is, the thrust and the drag forces on the wing at each time step are calculated using Eq. (16).

2.5 The calculation conditions

To easily compare the experimental results, the same calculation conditions were given as set in the experiment conditions of the visualization by Ro (2000). That is, the wing chord is set as $C=1$, uniform flow is $U=1$, movement velocity of the wing axis is $V=1$, the attack angle of the wing is $\alpha=30°$, the distance from the trailing edge of the wing to the wing axis r_p is $r_p=0.75C$, and the length, width and thickness of the water channel are $l=5.75C$, $h=2.5C$ and $0.02C$ respectively. Tsutahara et al. (1987) showed experimentally a higher thrust efficiency at the velocity ratio $V/U=1.0$ with the angle of attack $\alpha=30°$.

As expressed in the previous section, it was assumed that two flat plates and a wing in the flow field were installed, the surfaces of each object were represented with double panels, that is, with a finite number (M_b pieces) of source and vortex panels, where the panels of each object are

M_b=80.

In the present calculation, the time step size dt was set at dt=0.015 during the translating stage and as $dt_o = dt \times r_p C$ and $dt_c = dt \times (1 - r_p) C$ during the opening and closing stages. The results of the above procedure reveal the values for the time steps where the distances moved by the leading or trailing edges are all equal during the entire stroke.

3. Results and Discussion

Figure 3 shows the continuous flow pattern around the wing (NACA0010) during one stroke for Re=5900, the Reynolds number Re as defined by the wing chord and uniform flow. In Fig. 3, (a) refers to the numerical results of the streak lines and (b) represents the visualization photograph observed in the hydrogen bubble technique by Ro (2000) under the same conditions as in Fig. 3(a). In Fig. 3, 1 represents the opening stage; 2 to 4, the translating stage; and 5, the closing stage. The discontinuity of the streak lines seen in the vicinity of the trailing edge is due to the effects of the vortices generated at the trailing edge. Overall, the simulation results of the entire stroke match the visualized picture.

Figure 4 shows the streamlines (a) and the velocity vectors (b) around the wing during one stroke, under the same conditions as in Fig. 3. Here, considering the streamlines that passed the wing, we know that the flow goes around the wing, because streamlines bend to the moving direction of the wing at all stages and move together with the wing. The streamlines on the closed curve near both sides of the water channel were the effect of the vortex due to the occurrence of the reciprocating motion in the wing. As shown in the velocity vectors (b), the clockwise vortex existed at around the lower part of the wall, while the counter-clockwise vortex appeared near the upper part of the wall.

Figure 5 shows the results of the vortex distributions, the equi-vorticity contour and the isobaric lines, when the wing reached the center of the water channel from its start at the bottom wall. In the vortex distributions (a), the vortices shed from the wall surfaces of the water channel flowed downstream along the wall surface, the

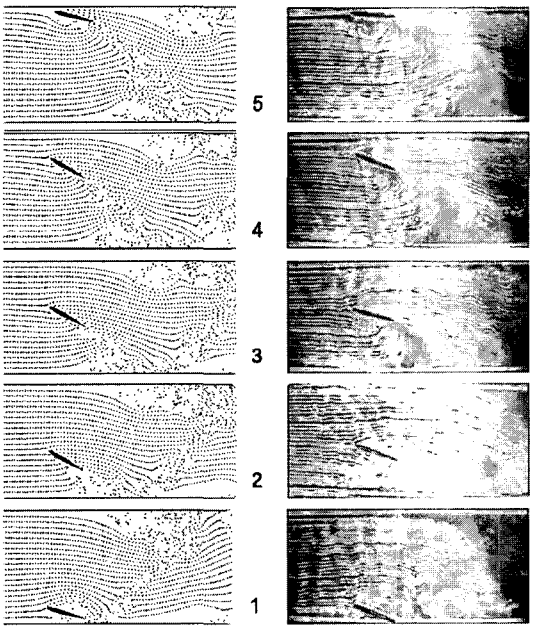

(a) Simulation (b) Photograph

Fig. 3 Streak lines for one stroke of the wing (C=1, h=2.5C, V/U=1.0, r_p=0.75C and α=30°)

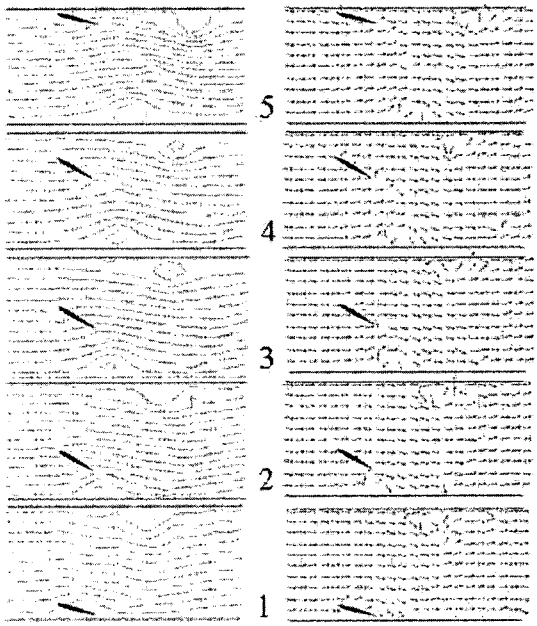

(a) Streamlines (b) Velocity vectors

Fig. 4 Flow patterns for one stroke of the wing

effect of a uniform flow. Furthermore, in the vortex distribution around the wing, the vortex shedding on the wing surface was separated at the trailing edge of the wing after it flowed along the surface of the wing. The separated vortex was mixed with the vortex shedding at the wall surface creating a complicated flow field, and the vorticity massed, as shown in the equi-vorticity contour (b).

Figure 6 shows the distribution of the pressure coefficient C_p on the surface of the wing. In Fig. 6, (a), (b) and (c) represent the opening, translating and closing stages, respectively. These correspond to positions 1, 3 and 5 in Figs. 3 and 4. Moreover, the 0.0 point on the horizontal axis for each figure corresponds to the p point in Fig. 1 and to the distance $r_p=0.75C$ from the trailing edge to the p point. The arrows show the directions of the pressure distribution, which moved in a counterclockwise direction starting from the trailing edge of the wing. Looking at the pressure distribution at the opening stage (a), the pressure coefficient in the backside for the uniform flow had a negative value from the trailing edge to the p point (the 0.0 point), while the pressure on the pressure side indicated almost a positive value except at the vicinity of the trailing edge. Contrarily, the pressure on the backside for the uniform flow had an almost negative value from the p point to the leading edge but showed a positive value on the pressure side. Considering the pressure distribution around the wing at the

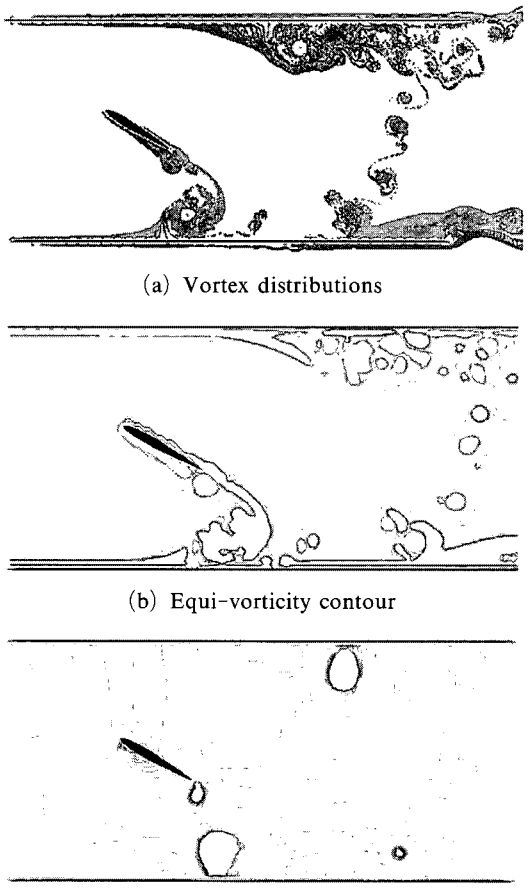

(a) Vortex distributions

(b) Equi-vorticity contour

(c) Isobaric lines

Fig. 5 Various flowfields at the point 3 of Fig. 3

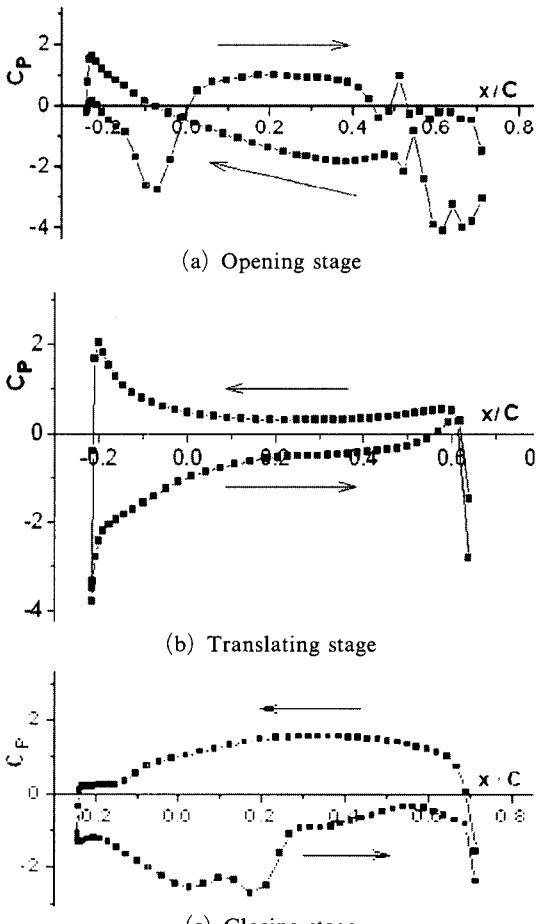

(a) Opening stage

(b) Translating stage

(c) Closing stage

Fig. 6 Pressure distribution around the wing ((a), (b) and (c) on the figure correspond to the points 1, 3 and 5 on Fig. 3)

translating stage (b), the pressure coefficient in the backside value for the uniform flow was almost positive, while the pressure on the pressure side showed a negative value. More significantly, it was also proven that the pressure difference between the pressure side and the backside appeared in the vicinity of the leading edge. Considering the pressure distribution at the closing stage (c), the pressure coefficient in the backside for the uniform flow had a positive value similar to that in the translating stage, while the pressure on the pressure plane had a negative value even as the pressure difference between the pressure side and the backside was not significant at the vicinity of the leading edge.

Figure 7 shows the time history of the thrust coefficient C_T at $\alpha=30$℃ and $V/U=1.0$. The horizontal axis in the figure represents the value that the moved distance of the wing axis is divided by the channel width. This value corresponds to the number of strokes. In Fig. 7, the solid lines represent the numerical results using this calculating method while the dashed lines are the experimental results measured by Ro (2000) under the same conditions. The reason that the experimental results have the large fluctuations is due to the surface wave generated by the movement of the wing, and particularly the larger fluctuations occurred in the early stage of each stroke is because the wing axis is instantaneously acted at the large force, due to the inertial force of the wing and the flow around the wing. In the opening stage, the thrust coefficient C_T shows a negative value for both the numerical and experimental results while in the translating stage, the numerical results show an increase as time passes. This trend is not analyzable from the experimental results due to severe fluctuation.

Figure 8 shows the numerical and experimental results of the drag coefficient C_D taken in the same conditions as in Fig. 7. The drag coefficient C_D also showed a fairly good match in the qualitative trend between the calculated and measured results. The drag coefficient C_D also gradually increased as the wing approaches the opposite wall, in which it started from a wall, though the experimental results can be undistinguishable

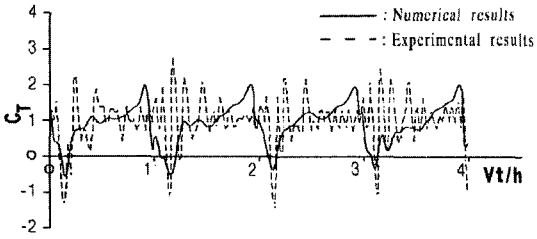

Fig. 7 Time variations for thrust coefficients

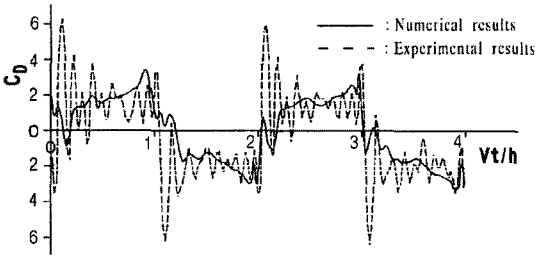

Fig. 8 Time variations for drag coefficients

due to the large fluctuations. The mean values of thrust coefficient and the drag coefficient were approximately 1.0 and 2.0 respectively at both the solid and the dashed lines of Figs. 7 and 8, and the numerical results were also quantitatively compatible with the experimental results.

In Figs. 7 and 8, the reason why the numerical results (solid lines) do not coincide with the experimental results (dashed lines), except the large fluctuations described the above, is considered that in the analytical model of Fig. 1 the flow surrounding the wing was assumed as 2-dimensional while in the actual experiment the free surface above the wing would affect the flow around the wing making it not thoroughly 2-dimensional.

4. Conclusions

This research simulated the velocity and pressure fields of a Weis-Fogh type ship propulsion mechanism using an advanced vortex method. The wing and water channel were presented through a finite number of source and vortex panels, and the vortex shedding was taken from the entire surface of each object. Both the velocity and the pressure field were evaluated with integral equations. The analyzed results are summarized as follows :

(1) The vortices which rotated in opposite directions near the two walls of the water channel were generated along the reciprocating motion of the wing.

(2) The pressure distribution on the wing surface was shown to have entirely different characteristics during the opening stage, the translating stage and the closing stage.

(3) The coefficients of the thrust C_T and the drag C_D gradually increased as the wing approaches the opposite wall from which it started.

References

Kamemoto, K., 1995, "On Attractive Features of the Vortex Methods," *Comp. Fluid Dyn. Rev. 1995 ed*. Hafez, M. & Oshima, K. JOHN WILEY & SONS., pp. 334~353.

Leonard, A., 1980, "Vortex Methods for Flow Simulations," *J. Comp. Phys*., Vol. 37, pp. 289~335.

Lighthill, M. J., 1973, "On the Weis-Fogh Mechanism of Lift Generation," *J. Fluid Mech*, Vol. 60, pp. 1~17.

Ro, K. D., 2000, "Calculation of Thrust and Drag Characteristics for Ship's Propulsion Mechanism of Weis-Fogh Type," *KSME Intl. J*., Vol. 14, No. 11, pp. 1249~1258.

Tsutahara, M. and Kimura, T., 1987, "An Application of the Weis-Fogh Mechanism to Ship Propulsion," *Trans. ASME J. Fluids Eng*., Vol. 109, pp. 107~113.

Tsutahara, M., Kimura, T. and Ro, K. D., 1989, "Ship Propulsion Using the Weis-Fogh Mechanism," *Bull. Mari. Eng. Soc.(in Japan)*, Vol. 17, No. 2, pp. 49~55.

Uhlman, J. S., 1992, "An Integral Equation Formulation of the Equation of Motion of an Incompressible Fluid," *Naval Undersea Warfare Center T.R*., pp. 10~086.

Weis-Fogh, T., 1973, "Quick Estimates of Flight Fitness in Hovering Animals, Including Novel Mechanism for Lift Production," *J. Exp. Bio*., Vol. 59, pp. 169~230.